Automated Robotic Microinjection of the Nematode Worm *Caenorhabditis elegans*

Xianke Dong, Pengfei Song, and Xinyu Liu, *Member, IEEE*

***Abstract*— The nematode worm *Caenorhabditis elegans* is a model organism widely used in biological research on genetics, development, neuroscience, and aging. Microinjection is an effective and widely adopted method to create transgenetic worms, perform ribonucleic acid (RNA) interference of certain genes, and introduce different types of molecules into specific locations inside a worm body. Based on microfluidics and robotic micromanipulation techniques, we develop a robotic system for automated microinjection of *C. elegans* with greatly improved injection speed and success rate over traditional manual microinjection. A double-layer microfluidic device with computer-controlled pneumatic valves is developed for automated on-chip loading, immobilization, injection, and downstream sorting of single worms. A new autofocusing-based contact detection algorithm is proposed to find the optimal injection position along the depth direction of the microscope field of view. The direction and location of the needle tip are reliably identified using an image processing algorithm. Through experiments on 240 worms, the system demonstrates automated injection at a speed of 6 worms/min (9.97 s/worm) with a presorting operation success rate of 78.8% (postsorting operation success rate: 100%), which are more than 23 times faster and 1.6 times higher than the speed (0.25 worm/min) and success rate (30%) of a proficient human operator, respectively. With the superior performance, this system will enable new large-scale gene- and molecule-screening studies on *C. elegans* that cannot be fulfilled by the conventional microinjection technique.**

***Note to Practitioners*—In the worm biology community, there are thousands of research laboratories worldwide that routinely cope with worm microinjection experiments. This article aims to present the functionality and performance of our automated robotic system for high-speed worm injection. Using the robotic system, a large number of *C. elegans* can be loaded into the microfluidic device for continuous worm immobilization and injection. A user-friendly graphical user interface (GUI) is developed to allow an operator to monitor the injection process on a computer screen, select the injection location inside the worm body (through computer mouse clicking), and direct the system (through keyboard input) for downstream sorting of the successfully injected worms for further culture. Given its unique features, such as high injection speed, high level of automation, and high success/survival rates, this system holds great potential to liberate worm researchers from the tedious manual injection process and provide unparalleled injection throughput and consistency.**

***Index Terms*— *C. elegans*, image processing, microfluidics, microinjection, robotic micromanipulation.**

I. Introduction

THE nematode worm *C. elegans* has been widely used as a model organism for investigating how various gene products function at specific tissue, cellular, and synaptic foci and how foreign molecules/chemicals affect the worm's biological pathways [1]. These studies are usually realized by injecting genetic materials or chemicals into the worm body to either suppress the expression of certain genes or perturb specific biological pathways [2]. To guarantee that the required phenotype demonstrated in the child generation, usually, a large number of adult worms are injected at the father generation. In worm biology laboratories, the required worm injection task is conducted manually. It takes a few hours for a proficient operator to prepare the facilities and perform injection for only a limited number of *C. elegans*, and the low throughput limits many biological studies that require large-volume worm injection. Furthermore, the inconsistent human operation leads to low success and survival rates of worm injection. All of these limitations call for the development of automated worm injection systems.

To reduce the human intervention level and improve the operation consistency of biomicroinjection, in the past two decades, numerous robotic systems have been proposed for the injection of either suspended cells (e.g., embryo and oocyte) or adherent cells (e.g., Hela cell, fibroblast, and endothelial cell) [3]–[13]. For instance, based on vision-based membrane tension estimation, a force-controlled robotic system has been developed for microinjection of zebrafish embryos [7]. Automated microinjection systems have also been reported for

Manuscript received September 20, 2018; revised November 19, 2019; accepted March 27, 2020. This article was recommended for publication by Associate Editor A. Julius and Editor D. O. Popa upon evaluation of the reviewers' comments. This work was supported in part by the National Sciences and Engineering Research Council of Canada under Grant RGPIN-2012-418553 and Grant RGPIN-2017-06374, in part by the Fonds québécois de la recherche sur la nature et les technologies under Grant 2013-NC-166238, in part by the Canada Foundation for Innovation under Grant 30316, and in part by the Canada Research Chairs Program under Grant 950-228836. The work of Xianke Dong and Pengfei Song was supported by the China Scholarship Council. *(Xianke Dong and Pengfei Song contributed equally to this work.) (Corresponding author: Xinyu Liu.)*

Xianke Dong was with the Microfluidics and BioMEMS Laboratory, Department of Mechanical and Industrial Engineering, University of Toronto, Toronto, ON M5S 3G8, Canada, and also with the Department of Mechanical Engineering, McGill University, Montreal, QC H3A 0C3, Canada.

Pengfei Song is with the Department of Electrical and Electronic Engineering, Xi'an Jiaotong–Liverpool University, Suzhou 215123, China.

Xinyu Liu is with the Microfluidics and BioMEMS Laboratory, Department of Mechanical and Industrial Engineering, University of Toronto, Toronto, ON M5S 3G8, Canada (e-mail: xyliu@mie.utoronto.ca).

This article has supplementary downloadable material available at http://ieeexplore.ieee.org, provided by the authors.

Color versions of one or more of the figures in this article are available online at http://ieeexplore.ieee.org.

Digital Object Identifier 10.1109/TASE.2020.2990995

high-speed injection of zebrafish and mouse embryos, in which a vacuum-based immobilization mechanism was proposed for immobilization many cells into a regular pattern [5], [10]. Different from single cells, alive *C. elegans* worms swim in solution or crawl on an agar plate, and the existing cell immobilization mechanisms cannot be directly applied to worm immobilization. Thus, effective worm immobilization mechanisms suitable for continuous robotic worm injection must be developed to overcome the bottleneck of automated worm injection.

Targeting automated worm injection, a few worm immobilization devices and injection systems have been reported to facilitate *C. elegans* microinjection [14]–[17]. An open-channel microfluidic device was developed [14], which immobilizes single worms using a vacuum-channel array. The operation of the device is relatively complex and was conducted manually; this makes the device incapable of conducting continuous loading and immobilization of many worms with high reliability. Furthermore, the cell injection procedure used in this work was not automated, that is, the regulation of the flow rate within the microchannel and the adjustment of the needle tip position were both conducted manually. In addition, because of the complex procedure designed for worm immobilization, this system has limited potential for large-scale robust injection. Another nanomanipulation system was reported by Nakajima *et al.* [15], [16] to deliver nanobeads into the worm body within an environmental scanning electron microscope (E-SEM). However, the E-SEM still cannot provide a completely biocompatible environment for fluid injection of live *C. elegans* due to its radiation and vacuum environment. Recently, a new worm immobilization method has been proposed for *C. elegans* microinjection, which employs temperature-sensitive hydrogel to immobilize the worm inside it [17]. The problem of this method is that the immobilized worms are randomly scattered inside the hydrogel with random orientations. The search of the worms takes additional time, and the injection has to be performed along different injection angles (the angle between the injection needle and the worm body); these factors, to some extent, limit the system's operation efficiency and consistency.

Combining microfluidics and robotic micromanipulation techniques, we propose a new robotic system for automated, high-throughput injection of *C. elegans*. A microfluidic device, with six computer-controlled pneumatic valves, is developed for automatic loading, immobilization, and postinjection collection of single worms at a high speed. Before each injection experiment, the system performs rapid and automatic preparation, including: 1) determination of the vertical position of the injection needle (along the depth direction of the microscope view) for worm injection, through an autofocusing-based contact detection algorithm; 2) detection of the in-plane position (in the image frame) of the needle tip using a reliable image processing algorithm; and 3) calibration of the coordinate transformation between the image frame and the robot frame. During an experiment, the system visually monitors the operation of the microfluidic device and correspondingly controls the on-chip valves and the injection robot to realize automatic worm injection. Injection experiments on 240 *C. elegans* worms are performed to fully test the system performance. This article is an extension of a previous conference paper [18]. In this journal version, we include a new and more robust contact detection algorithm, more technical details of the system setup and operation, a detailed description of the needle tip recognition algorithm, and more experimental results (i.e., a much larger sample size of robotic worm injection and additional survival testing results of the injected worms).

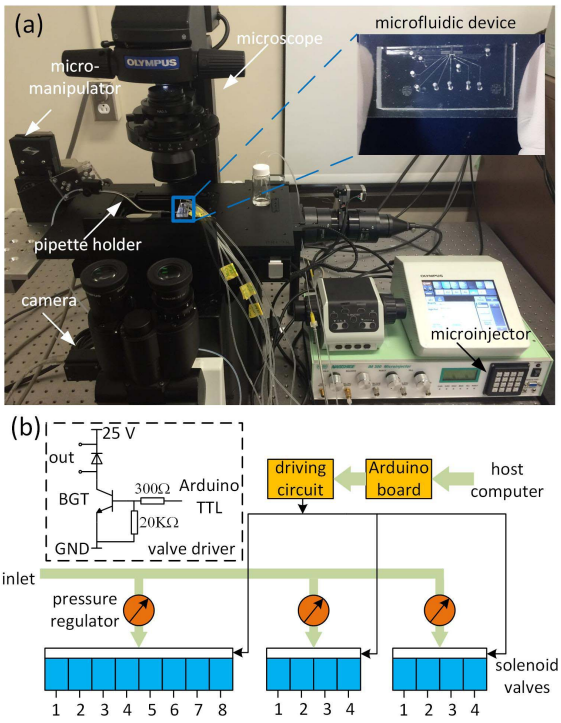

Fig. 1. Setup of the robotic injection system. (a) Photograph of the system. (b) Schematic of the pressure unit for actuating on-chip valves of the microfluidic device.

II. Robotic Worm Injection System

A. System Setup

The robotic worm injection system, as shown in Fig. 1(a), consists of an inverted microscope (IX83, Olympus) with a 4× objective (NA: 0.13) for sample imaging, a microfluidic device with on-chip valves for worm immobilization and sorting, a three-degree-of-freedom (3-DOF) micromanipulator (MP285, Sutter) mounted with an injection needle for worm injection, a pressure-driven microinjector (IM-300, Narishige) connected with the injection needle for delivering a foreign material into the worm body, a motorized XY stage (ProScan III, Prior) for carrying the microfluidic chip under the field of view (FoV) of the microscope, a custom-made, computer-controlled pressure unit to regulate the operation of valves on the microfluidic device, and a host computer (3.1-GHz CPU and 8-GB RAM) for system control. A COMS camera (Basler, A601f) mounted on the microscope is used to provide the visual feedback for the system.

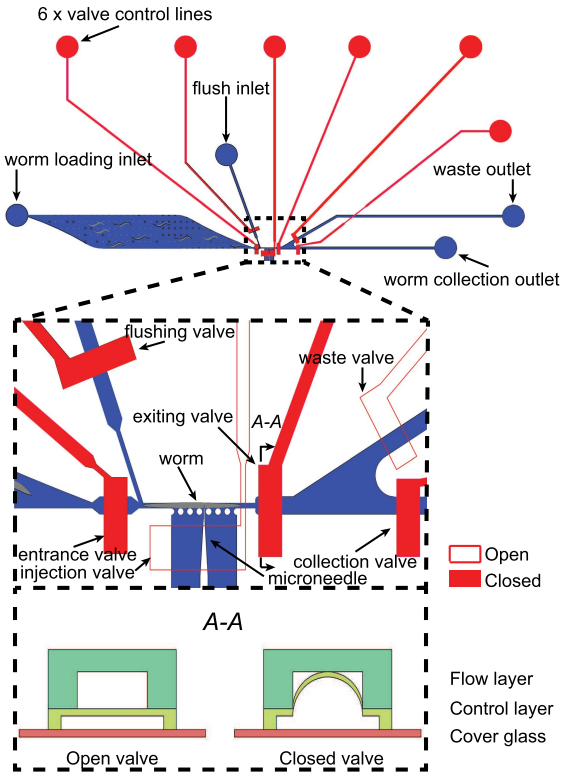

Fig. 2. Schematic of the microfluidic device for worm immobilization.

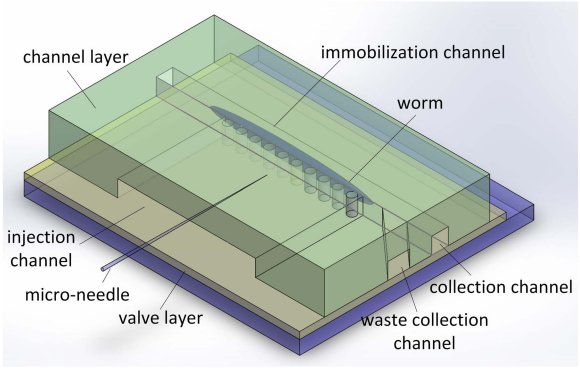

Fig. 3. Detailed structure of the injection and immobilization channels.

The custom-made pressure unit, as schematically shown in Fig. 1(b), consists of 16 solenoid valves (S10MM-30-24-2/A, Pneumadyne Inc.), three manually adjustable pressure regulators (ARG20-N01G1-Z, SMC Pneumatics), a pressure inlet connected to a compressed nitrogen gas tank (output pressure: 85 psi), a driver circuit board for the 16 solenoid valves, and a microcontroller unit (Arduino UNO) connected with the host computer. The pressure unit could provide pressure sources in the range of 0–80 psi and at three different levels, to actuate on-chip pneumatic valves whose operations require different pressure levels. The driver circuit for a single valve is also shown in Fig. 1(b).

B. Microfluidic Device Design

The double-layer microfluidic device was designed for rapid single-worm loading, immobilization, and postinjection sorting. The device design, fabrication, and operation have been reported previously [19]. To make this article self-contained, we briefly introduce its design here.

The device has 30-μm-tall rectangular control channels (red in Fig. 2) on the bottom layer and 45-μm-tall flow channels (blue in Fig. 2) on the top layer, and was fabricated from polydimethylsiloxane (PDMS) using standard multilayer soft lithography [20]. Based on their functions, the device channels can be mainly divided into three regions: 1) a loading chamber; 2) immobilization/injection channels; and 3) downstream sorting channels. The loading chamber includes a micropillar array, and the spacing between adjacent micropillars is 300 μm, which is effective to filter out debris in the worm culture medium and allow the young adult worm to swim through. This design avoids clogging of the immobilization channel and, thus, improves the reliability of device operation. The immobilization channel is 1200-μm long and 40-μm wide, which is slightly narrower than the diameter of a young adult worm (40–60 μm). The plug of a worm in the immobilization channel will significantly increase the channel's flow resistance, keeping another worm from entering.

An open-ended injection channel is perpendicularly connected to the immobilization channel, allowing an injection needle to be inserted through the open end of the injection channel and reach the immobilization channel (Fig. 3). A row of micropillars (diameter: 40 μm and pitch: 115 μm) is arranged at the junction of the immobilization and injection channels, which restricts an immobilized worm from swimming into the injection channel and, in the meanwhile, allows the needle to reach the worm body for injection. The width of the injection channel is set to be 800 μm, which covers the majority of the worm body for injection. A bifurcated channel is connected to the downstream of the immobilization channel and regulated by two valves for post-injection worm sorting.

III. Experimental Procedure

A. System Preparation

Before each injection experiment, a microfluidic device, loaded with a batch of 40 worms, is first mounted onto the XY stage of the microscope. An injection needle loaded with injection material is then mounted on the micromanipulator horizontally (at 0° tilting angle), with its tip in the microscope FoV and above the PDMS substrate outside the injection channel of the microfluidic device ("contact detection area" in Fig. 5). Fig. 4 shows the overall flow of the system preparation and automated robotic injection. The system initiates the automatic preparation process by controlling the needle to contact the PDMS substrate, during which the vertical position (along the depth direction of the microscope FoV) of the needle–substrate contact point is detected using an autofocusing-based contact detection algorithm (see Section IV-A). After that, the needle tip is automatically lifted to the vertical level of 22.5 μm (half of the injection channel height) above the PDMS surface, and the microfluidic device is moved toward the needle to insert the needle tip into the injection channel and

TABLE I
OPERATION STATES OF THE MICROFLUIDIC DEVICE

System states	loading inlet	flushing inlet	entrance valve	injection valve	collection valve	exiting valve	flushing valve	waste valve
Worm loading state	on	off	on	off	off	partially off	off	on
Worm injection state	off	off	off	on	off	off	off	on
Worm collection/discard state	off	on	off	off	on	on	off/on	on/off

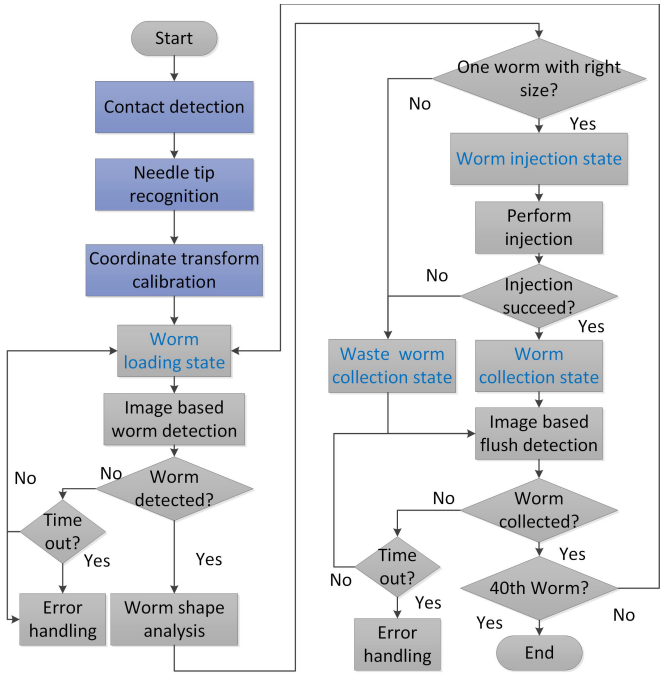

Fig. 4. Flowchart of the robotic worm injection procedure.

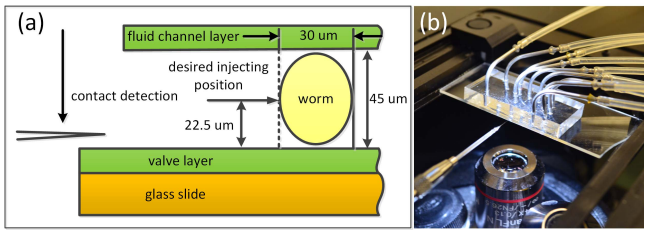

Fig. 5. Autofocusing-based contact detection. (a) Schematic of determining the vertical injection position through contact detection. (b) Photograph of configuration of the injection needle and the photograph during contact detection.

place the injection and immobilization channels into the FoV. During the subsequent injection process, the vertical position of the needle tip remains the same, and its in-plane position is controlled inside the injection channel for worm injection.

Once the needle tip is moved into the injection channel, the tip position in the image coordinate frame is accurately detected using a tip recognition algorithm (see Section IV-B). To control the needle movement in the image coordinate frame, the mapping between the image coordinate frame (in pixels) and the micromanipulator coordinate frame (in μm) is calibrated automatically (see Section IV-C). Note that this automatic coordinate mapping process needs to be conducted every time a new injection needle is mounted onto the micromanipulator to compensate for the subtle difference in the needle length and alignment. Video 1 in the Supplementary Material shows the entire system preparation process.

B. Overall Injection Procedure

The control flow of the automatic injection process (see Fig. 4) was designed to maximize the parallelization level of different steps and, thus, increase the system efficiency. Table I summarizes the operation states of all the microfluidic valves and supplied pressures during the entire worm injection process.

To start the automatic injection, on-chip valves of the microfluidic device are set to the "worm loading state" (see Table I), and the constant pressure of 10 psi is applied to the worm loading inlet to sequentially drive individual worms into the immobilization channel. At this stage, the entrance and waste valves are fully opened, while the existing valve is partially closed and other valves are kept closed. With a pressure-driven flow from the device inlet, a worm can be loaded into the immobilization channel. Once an immobilized worm is detected through image processing (see Section IV-D), the entrance valve and the inlet driving pressure are automatically switched OFF to minimize flow-induced worm movements during injection, and the injection valve is opened ("worm injection state" in Table I) to allow the needle to reach the immobilized worm.

Depending on the type of study requiring *C. elegans* injection, the location to deliver the injection materials inside the worm body could be different. The robotic system allows the user to identify the in-plane image coordinates of the target location on the computer screen through computer mouse clicking and then controls the injection needle to penetrate the worm body and deliver a controlled amount of injection material to the desired location. If the material delivery is successful, the worm body will slightly expand along its longitudinal direction (see Video 2 in the Supplementary Material). We have experimentally verified that this is a reliable indicator for a successful injection (see data in Section V-A). During injection, the user readily monitors the elongation of the worm body upon material delivery on the computer screen and indicates to the system, through keyboard input, whether the current injection is successful. After injection, the injection valve is closed, and the existing valve is opened. The pressure source connected to the flush inlet is turned on, and the flush

valve is opened so that the worm could be flushed out of the immobilization channel. For a successful injection, the worm collecting valve is opened to guide the injected worm to the collection outlet; otherwise, the waste valve is opened to let the worm reach the waste outlet ("worm collection/discard state" in Table I). When the worm is visually detected to be flushed out of the immobilization channel, the system is switched back to the "worm loading state," and the next worm is loaded. This process is repeated until all the worms loaded to the device are injected. Video 2 in the Supplementary Material shows the automatic injection process.

IV. System Automation Techniques

A. Autofocusing-Based Contact Detection

In this system, the injection needle is required to be operated in the injection channel in the top layer of the microfluidic device, as shown in Fig. 5. As a result, the vertical position of the needle is a critical factor that significantly influences the injection success rate since injecting either the upper or lower portion of the worm body will increase the risk of needle tip slipping on the worm body (Fig. 5). Thus, the optimal vertical level of the needle tip for injection is the middle position of the channel height (Fig. 5).

A contact detection mechanism was developed based on Tenenbaum's autofocusing algorithm [21], [22] to detect the vertical position at which the needle tip contacts with the PDMS substrate. To improve the contact detection accuracy, a 40× objective was automatically switched into the optical path for imaging, providing a shallow depth of field of 2.2 μm. The image is first focused, through the microscope z-motor, on the PDMS substrate where the contact will take place. The injection needle tip, initially a few hundreds of micrometers above the PDMS substrate, is then lowered toward the PDMS substrate at a constant speed of 10 μm/s, during which its in-focus level is evaluated by calculating the following focus objective function:

$$F = \sum_{\mathrm{ROI}_x} \sum_{\mathrm{ROI}_y} (S_x(x, y)^2 + S_y(x, y)^2) \tag{1}$$

where $S_x(x, y)$ and $S_y(x, y)$ are the convoluted images by the Sobel operators. As the injection needle tip is mounted horizontally, its in-focus image reveals sharp and clear edges, leading to the maximum focus objective function. The contact detection algorithm records the vertical position of the needle tip from which the needle tip image becomes in-focus, which corresponds to the vertical contact point of the tip and the substrate.

Fig. 6 shows an image sequence [see Fig. 6(a)] of the needle tip captured during contact detection and the corresponding values [6(b)] of the focus objective function as a function of the needle vertical position Z_m (in the micromanipulator frame). When the needle tip is out of focus, only its blurred shadow can be observed [P1 and P2 in Fig. 6(a)]. The objective function F gradually increases as the tip moves toward the focal plane [see Fig. 6(b)]. Once the contact occurs, F remains at a relatively stable level [P3–P4 in Fig. 6(a)] since the PDMS surface constrains the needle tip from lowering further. Our

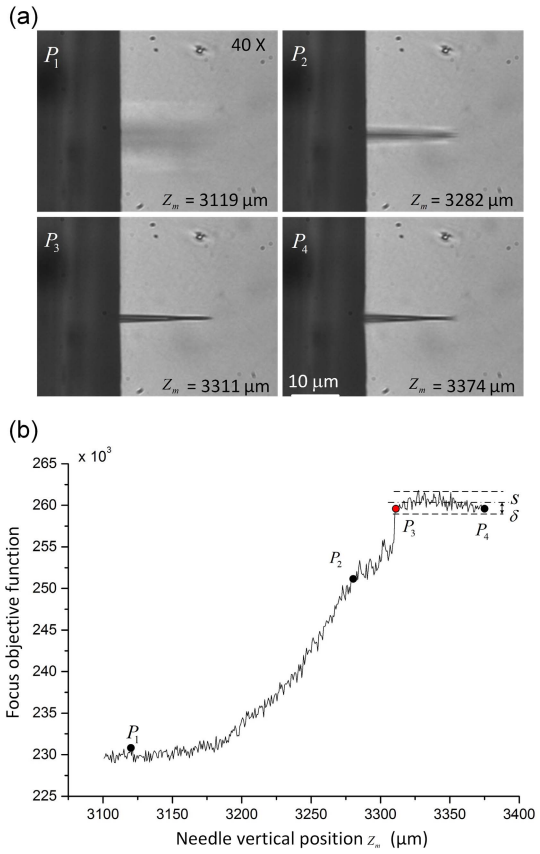

Fig. 6. Experimental results of autofocusing-based contact detection. (a) Image frames of the needle tip at 40× at four different vertical positions. (b) Focus objective function versus needle vertical position.

algorithm automatically detects the starting point of the stable level [P3 in Fig. 6(a)] and records the corresponding vertical contact position z_{mc}

$$Z_{\mathrm{mc}} = \arg\min_{Z_m} \{F(Z_m) \geq \bar{s} - \delta\} \tag{2}$$

where $\bar{s}$ and δ are the average and standard deviation of the focus objective function in its stable level [P3–P4 in Fig. 6(a)], respectively. With the same microscope illumination condition, the threshold of $\bar{s} - \delta$ was found to remain at a stable value and, thus, is effectively for determining the vertical contact position Z_{mc}. Compared with the intensity-based contact detection algorithm proposed in our previous system in [18], this algorithm is evaluating the focus level of the entire ROI and, therefore, less sensitive to pixel intensity noises and slight vibrations of the moving micromanipulator. Thus, it has been tested to be more reliable and also robust to illumination changes.

Ignoring the small contact-induced deformation of the PDMS substrate, the optimal vertical position for worm injection is defined as 22.5 μm (half of the injection channel height) above the vertical contact position (see Fig. 5). The needle tip is then lifted to the optimal injection position, and the microfluidic device is moved toward the needle tip to insert it into the injection channel. In the meanwhile, the immobilization channel is moved into the FoV.

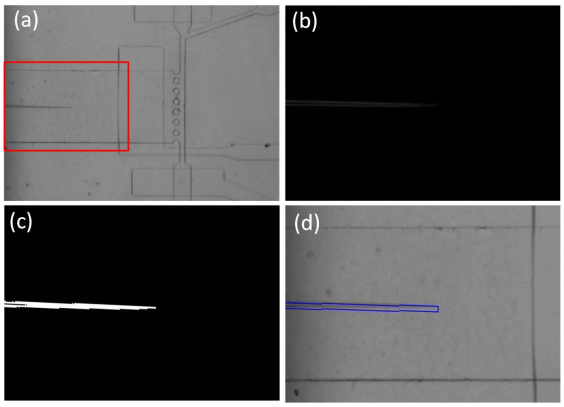

Fig. 7. Image processing frames for needle tip recognition. (a) Raw image with the region of interest (ROI) highlighted. (b) ROI image with background removed. (c) Binarized image of the ROI after adaptive thresholding. (d) ROI image with the recognized needle area.

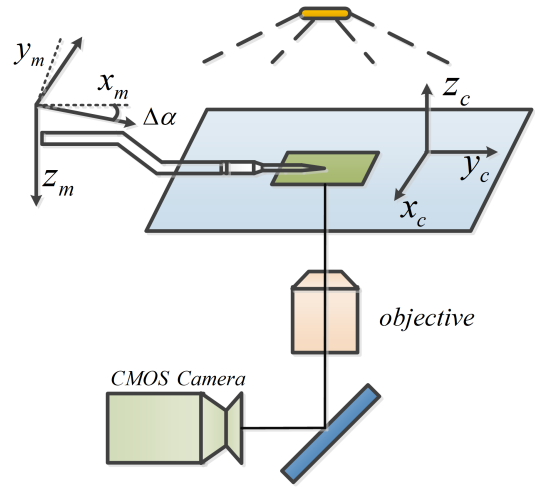

Fig. 8. Coordinate frames of the robotic system.

B. Visual Detection of the Needle Tip

After contact detection, image coordinates of the needle tip need to be visually recognized for coordinate mapping between the micromanipulator frame and the image frame. To acquire a background image of the injection channel, the needle tip is temperately moved out of the channel, the system grabs a background image from the camera, and the needle tip is moved back to its initial position inside the injection channel (see Video 1 in the Supplementary Material). Then, a region of interest (ROI), including the needle tip [the red rectangle in Fig. 7(a)], is selected by the user on the computer screen, and the tip recognition algorithm is applied to the selected ROI. The current ROI is subtracted by the corresponding portion of the previously grabbed background image to eliminate the background features, and the resultant image is shown in Fig. 7(b). A Gaussian blur operator is applied to the resultant image to reduce the image noises. The dimension of the blur operator is selected to be 3 to avoid eroding the edge of the needle.

The denoised ROI is binarized through Otsu adaptive thresholding to identify the needle tip region [see Fig. 7(c)]. Canny edge detection followed by rotated rectangle pattern fitting is then applied to the obtained binary ROI, and the fit rectangle with the largest connected domain area is recognized as the needle area [see Fig. 7(d)]. The rightmost pixel of the recognized needle area is identified as the needle tip.

C. Coordinate Transformation Calibration

In order to control the in-plane motion of the needle tip based on the visual feedback, the coordinate transformation between the image frame and the micromanipulator frame needs to be routinely performed. Considering the existence of small misalignments between the micromanipulator frame and the camera frame, we proposed a linear-regression-based calibration method to accurately determine the mapping relationship between the two frames.

As illustrated in Fig. 8, the micromanipulator frame $x_m - y_m - z_m$ and the image frame $x_i - y_i$ have a small misalignment. Considering only in-plane motions of the needle tip during worm injection, it is easy to obtain that

$$P_m = kA^{2\times 2}P_i + B^{2\times 1} \tag{3}$$

where k is a magnification scalar and A is an orthogonal matrix subject to $A^TA = I$. $P_m = [x_m, y_m]^T$ and $P_i = [x_i, y_i]^T$ are the projected coordinates of a point in the micromanipulator frame and the camera frame, respectively. Here, we denote kA as $\bar{A}$ for simplicity.

To calibrate the coordinate mapping, the needle tip is moved by small displacements to multiple positions within the injection channel, and the system records in-plane coordinates of the tip's positions in: 1) the micromanipulator frame (from the position feedback of the micromanipulator): $(x_{m1}, y_{m1}), \ldots, (x_{mn}, y_{mn})$ and 2) the image frame (through visual recognition of the needle tip): $(x_{i1}, y_{i1}), \ldots, (x_{in}, y_{in})$. The parameter n is the number of tip positions. Then, the coefficient matrices of coordinate transformation B and $\bar{A}$ can be determined by

$$\begin{bmatrix} B & \bar{A} \end{bmatrix}^T = (X^TX)^{-1}X^T\begin{bmatrix} P_x & P_y \end{bmatrix} \tag{4}$$

where

$$P_x = \begin{bmatrix} x_{m1} & x_{m2} & \ldots & x_{mn} \end{bmatrix}^T \tag{5}$$

$$P_y = \begin{bmatrix} y_{m1} & y_{m2} & \ldots & y_{mn} \end{bmatrix}^T \tag{6}$$

$$X = \begin{bmatrix} 1 & x_{i1} & y_{i1} \\ \vdots & \vdots & \vdots \\ 1 & x_{in} & y_{in} \end{bmatrix}. \tag{7}$$

Note that all the recorded positions $(x_{i1}, y_{i1}), \ldots, (x_{in}, y_{in})$ should not be in a straight line, which ensures that $\text{rank}(X) = 3$ and X^TX is invertible. In our experiments, we moved the needle tip to a grid of 3×3 positions with a pitch of 115 μm and carried out the coordinate mapping calibration in real time. Once the calibration is completed, the system is ready for worm injection.

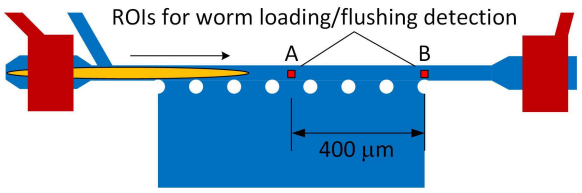

Fig. 9. Schematic of the ROIs inside the immobilization channel for visual detection of worm loading and unloading in the injection channel.

D. Visual Detection of Worm Loading and Unloading in the Immobilization Channel

During automated worm injection, the loading and unloading of a worm in the immobilization channel will be monitored by an image processing algorithm so that the on-chip valves can be activated accordingly to switch between different operation states (see Table I). The algorithm constantly monitors the average pixel intensities of two ROIs (10×10 pixels) in the immobilization channel (see Fig. 9). When a worm is loaded into the injection channel, its body will fill the two ROIs and makes their average intensities significantly decrease (because of the darker worm body than channel background). By comparing the current average intensities of the two ROIs with that of the channel background, the loading and unloading of the worm can be detected.

The worm loading and unloading events are defined by the following two inequalities, respectively,

$$\frac{1}{4s^2}\sum_{R_x-s}^{R_x+s}\sum_{R_y-s}^{R_y+s}(I_0(x,y)-I(x,y)) > \delta_1 \tag{8}$$

$$\frac{1}{4s^2}\sum_{R_x-s}^{R_x+s}\sum_{R_y-s}^{R_y+s}(I_0(x,y)-I(x,y)) < \delta_2 \tag{9}$$

where I_0 and I are background image and current image correspondingly. (R_x, R_y) refers to the position of selected ROI in image frame. δ_1 and δ_2 are experimentally determined thresholds. $s = 5$ in the experiment.

We selected the two ROIs in the middle (ROI-A) and right-end (ROI-B) positions of the immobilization channel (see Fig. 9), and the coordinates of the ROIs were entered into the system by simply mouse clicking the corresponding points on the screen monitor in our software graphical user interface (GUI). When the average intensities of both ROIs decrease by a value larger than a threshold, it indicates a worm has been completely loaded into the immobilization channel. The recovery of the ROI average intensities back to its original background value means that the worms have been flushed out of the immobilization channel. Monitoring the average intensities of the ROIs avoids any false worm detection caused by small particles passing through the ROIs. Under the illumination that we used in our experiments, the average intensity of each ROI drops by 120–150 for most worms. Leaving some quantity margins, $\delta_1 = 80$ and $\delta_2 = 30$ were used in our experiments.

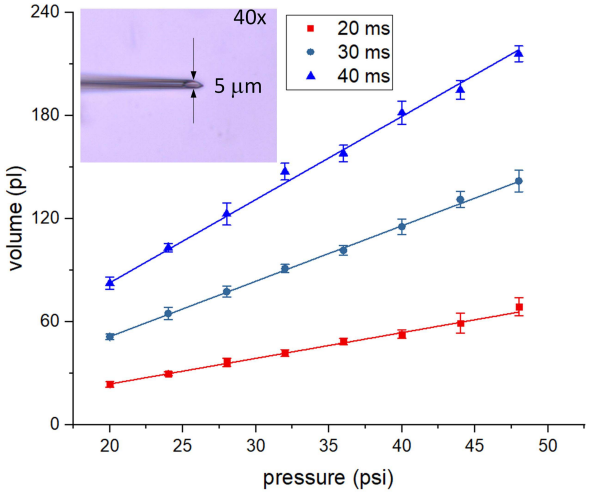

Fig. 10. Calibration results of the injection volume as functions of injection pressure and pressure pulsewidth.

E. Injection Volume Control

The delivered volume of injection material is determined by the injection pressure level, the pressure pulse duration, and the diameter of the needle tip. The injection volume control is critical to achieve consistent biological results from the injected worms and can also enable the quantitative study of dose effect on specific biological processes of the injection worm. Using a needle tip with typical outer and inner diameters of 5 and 3.5 μm, respectively, we calibrated the injection volume as a function of the pressure level and the pressure pulse duration. Deionized water was used as the injection sample for volume calibration. By supplying a short pressure pulse to the injection needle, a small spherical water drop was delivered into mineral oil, and the shape of the water drop was immediately measured at $10\times$ using the Hough circle pattern fitting. Fig. 10 shows the experimental results of injection volume calibration ($n = 5$).

F. Worm Culture and Preparation

The *C. elegans* used in our experiments was wild type N2 strain cultured using on a standard procedure [23]. Microinjection is usually performed on young adult worms, and we synchronized young adult worms by culturing worm embryos for 54 h at 20 °C on agar plates seeded with OP50 *E. coli* [19]. Before injection, the young adult worms with diameters of 35–40 μm were selected and sequentially transferred into three droplets of M9 medium to wash off the *E. coli* and other small impurities from their bodies and finally loaded into the inlet of the microfluidic device using a pipette. All the young adult worms were injected within 30 min after they were transferred from the culture plate.

V. Experimental Results and Discussion

A. Experimental Results

In the experiments, FITC fluorescent dye was first injected to visualize the material delivery into the worm body through fluorescence imaging. The injection/retraction speeds were both 5000 μm. By applying a 30-ms pulse of 31-psi pressure

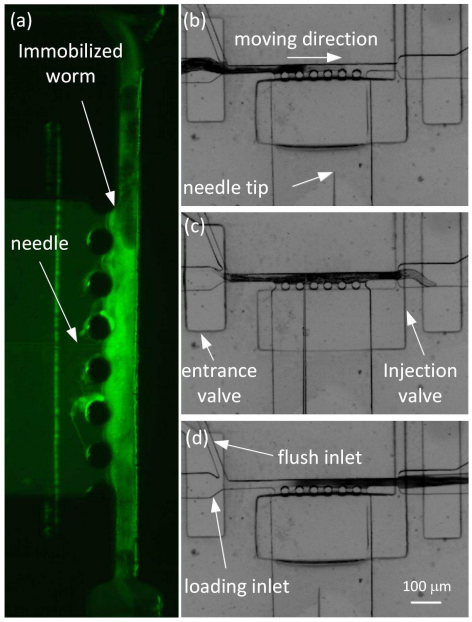

Fig. 11. Photographs of the worm injection process. (a) Fluorescent image of the worm body right after fluorescent dye is delivered. (b) Worm loading. (c) Worm immobilization and injection. (d) Worm flushing after injection.

to the injection needle (inner diameter: 3.5 μm), 85 pl of FITC dye was injected into the worm body. As shown in Fig. 11(a), the fluorescence intensity of the proximity of the injection location inside the worm body is much higher than that of the channel background, indicating successful delivery of the FITC dye. Note that the injection channel also shows a low green fluorescence because of the diffusion of FITC dye from the needle tip into the injection channel. Upon the material delivery, it was also observed that the worm body expanded along its longitudinal direction (see Video 2 in the Supplementary Material). To verify if the worm body expansion could be used as a reliable indicator for material delivery, another 20 worms were injected with the FITC dye, and the correlation of the worm body expansion and the successful material delivery was found in all the 20 injections. Thus, the worm body expansion upon injection was used in the following experiments to count the injection success rate.

To evaluate the system performance, deionized water was automatically injected into 240 worms (six batches and 40 worms/batch). The automated worm injection process was shown in Video 2 in the Supplementary Material. Two performance parameters were quantified based on the experiment data: injection speed and operation success rate. The success of injection was evaluated by visually observing the worm body expansion upon injection, and the operation success rate is defined as the ratio of the number of successfully injected worms (with body expansion) to the total number of injected worms.

The system demonstrated an average injection speed of 6 worm/min (average processing time: 9.97 s/worm) with an operation success rate of 78.8%, and these parameters are both superior over the performance of manual injection (speed: 0.25 worms/min, success rate: ∼30%; data provided by a proficient worm injection operator [24]). During injection, the user monitored the injection of each worm and instructs the

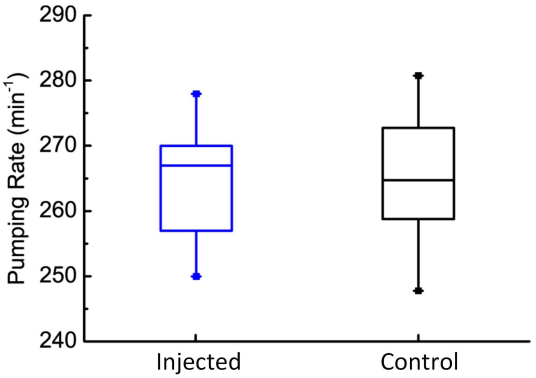

Fig. 12. Experimental results of the pharynx pumping rates of the injected worm group and the control group.

system (through keyboard input) whether or not the current injection was successful, and the system then sorted the successfully injected worms into the sample collection outlet of the microfluidic device. Therefore, the postsorting success rate is 100%, meaning that all the worms in the sample collection outlet were successfully injected. Among the average worm processing time of 9.97 s, the average worm loading, injection, and flushing times are 2.7, 5.51, and 1.76 s, respectively.

The failure modes of the system causing the 21.2% failed injections include: 1) no material delivery upon injection (no worm body expansion; 18.2%) and 2) simultaneous loading of two worms into the immobilization channel (3%). The unsuccessful material delivery could be possibly due to temporary clogging of the needle and/or nonpenetration of the worm body. The penetration rate can be improved by aligning the microneedle vertical to the target worm skin. The loading of two worms can be further alleviated by better size synchronization of the worms loaded into the microfluidic device.

From Video 2 in the Supplementary Material, one can observe that there is a small amount of lysis from the worm body upon retracting the injection needle. Accordingly, we also examined the potential physiological impact imposed on the injected worms through the measurement of the worm's pharynx pumping rate. The pumping rate of the worm pharynx corresponding to its food intake is an important measure of the worm's physiological condition. As shown in Fig. 12, the pumping rates measured from the injected worms are 240–280 pumps/min, which is in the common range of that of the wild type N2 worms [25]. In addition, the pumping rate data from the injected and control group do not reveal a significant difference ($p > 0.3$).

B. Discussion

In conventional worm injection, a young adult worm is transferred from the Petri dish to a glass slide under the microscope, on which a drop of oil is placed for worm immobilization. Then, a micromanipulator is controlled manually to inject the worm. The worm preparation and injection are both time-consuming and tedious and require significant training of the operator.

Our experiment on robotic injection of 240 *C. elegans* worms demonstrated that the developed system is capable

of automatically injecting worms at a speed of 9.97 s/worm with a presorting operation success rate of 78.8%. The high operation efficiency mainly results from the continuous and efficient worm loading and immobilization (2.7 s/worm). The time required for worm injection (5.5 s/worm) and sorting (1.76 s/worm) is longer than the worm loading time since the injection and sorting speeds are limited by several parameters, such as the maximum speed of the micromanipulator, the response time of the microfluidic valves, and the time required for the user to indicate a successful injection. In our experiments, the preparation time of contact detection and coordinate mapping (see Video 1 in the Supplementary Material) should also be counted into the average injection speed of worms. Considering a large number of injected worms in each experiment batch, this time portion is neglected in this article.

Note that human involvement is still needed to identify the injection location in the immobilized worm body and indicate a successful injection during the conscious operation of the system. Because of the round section shape, the worm orientation along the dorsal-ventral axis cannot be controlled during immobilization. As a result, it remains difficult to detect the worm gonad via computer vision since the morphology within the worm body varies for every individual worm. It is possible to integrate worm orientation control mechanisms into the microfluidic device [26], which could make the visual recognition of the worm gonad feasible. In addition, with a computer vision algorithm for detecting automatic skin penetration and delivery of external materials, the manual judgment for successful injection trails can also be further automated by a machine.

VI. Conclusion

We presented an automated robotic system for high-throughput injection of *C. elegans*. A vision-based contact detection algorithm was adopted to determine the optimal injection position along the z-axis. Based on the effective image processing algorithm, the needle tip was efficiently identified online from the microscope camera image for accurate position control. In addition, a multilayer PDMS device was designed to rapidly load, immobilize, flush, sort, and collect the worms. Experiments based on the injection of 240 worms showed that the system can perform *C. elegans* injection at a speed of 9.97 s/worm with an operation success rate of 78.8%.

Acknowledgment

The authors would like to thank Prof. Siegfried Hekimi and Prof. Michael Hendricks for their assistance in worm culture and handling.

References

[1] M. Rieckher, N. Kourtis, A. Pasparaki, and N. Tavernarakis, *Transgenesis Caenorhabditis elegans*. Totowa, NJ, USA: Humana Press, 2009, pp. 21–39, doi: 10.1007/978-1-60327-019-9_2.

[2] L. A. Berkowitz, A. L. Knight, G. A. Caldwell, and K. A. Caldwell, "Generation of stable transgenic *C. elegans* using microinjection," *J. Visualized Exp.*, vol. 15, no. 18, 2008, Art. no. e833.

[3] Y. Sun and B. J. Nelson, "Biological cell injection using an autonomous microrobotic system," *Int. J. Robot. Res.*, vol. 21, nos. 10–11, pp. 861–868, Oct. 2002.

[4] Z. Lu, P. C. Y. Chen, J. Nam, R. Ge, and W. Lin, "A micromanipulation system with dynamic force-feedback for automatic batch microinjection," *J. Micromech. Microeng.*, vol. 17, no. 2, pp. 314–321, Feb. 2007.

[5] W. Wang, X. Liu, D. Gelinas, B. Ciruna, and Y. Sun, "A fully automated robotic system for microinjection of zebrafish embryos," *PLoS ONE*, vol. 2, no. 9, p. e862, 2007.

[6] Y. Zhang, K. Kiong Tan, and S. Huang, "Vision-servo system for automated cell injection," *IEEE Trans. Ind. Electron.*, vol. 56, no. 1, pp. 231–238, Jan. 2009.

[7] H. B. Huang, D. Sun, J. K. Mills, and S. H. Cheng, "Robotic cell injection system with position and force control: Toward automatic batch biomanipulation," *IEEE Trans. Robot.*, vol. 25, no. 3, pp. 727–737, Jun. 2009.

[8] W. H. Wang, X. Y. Liu, and Y. Sun, "High-throughput automated injection of individual biological cells," *IEEE Trans. Autom. Sci. Eng.*, vol. 6, no. 2, pp. 209–219, Apr. 2009.

[9] A. Ghanbari, W. Wang, C. E. Hann, J. G. Chase, and X. Chen, "Cell image recognition and visual servo control for automated cell injection," in *Proc. 4th Int. Conf. Auto. Robots Agents*, Feb. 2009, pp. 92–96.

[10] X. Liu *et al.*, "Automated microinjection of recombinant BCL-X into mouse zygotes enhances embryo development," *PLoS ONE*, vol. 6, no. 7, 2011, Art. no. e21687.

[11] X. Liu, Z. Lu, and Y. Sun, "Orientation control of biological cells under inverted microscopy," *IEEE/ASME Trans. Mechatronics*, vol. 16, no. 5, pp. 918–924, Oct. 2011.

[12] H. Maruyama, N. Inoue, T. Masuda, and F. Arai, "Selective injection and laser manipulation of nanotool inside a specific cell using optical pH regulation and optical tweezers," in *Proc. IEEE Int. Conf. Robot. Autom. (ICRA)*, May 2011, pp. 2674–2679.

[13] Z. Ni, A. Bolopion, J. Agnus, R. Benosman, and S. Regnier, "Asynchronous event-based visual shape tracking for stable haptic feedback in microrobotics," *IEEE Trans. Robot.*, vol. 28, no. 5, pp. 1081–1089, Oct. 2012.

[14] X. Zhao, F. Xu, L. Tang, W. Du, X. Feng, and B.-F. Liu, "Microfluidic chip-based *C. elegans* microinjection system for investigating cell–cell communication *in vivo*," *Biosensors Bioelectron.*, vol. 50, pp. 28–34, Dec. 2013.

[15] M. Nakajima, T. Hirano, M. Kojima, N. Hisamoto, M. Homma, and T. Fukuda, "Direct nano-injection method by nanoprobe insertion based on E-SEM nanorobotic manipulation under hybrid microscope," in *Proc. IEEE Int. Conf. Robot. Autom.*, May 2011, pp. 4139–4144.

[16] M. Nakajima *et al.*, "Local nano-injection of fluorescent nano-beads inside *C. elegans* based on nanomanipulation," in *Proc. IEEE/RSJ Int. Conf. Intell. Robots Syst.*, Oct. 2012, pp. 3241–3246.

[17] C. L. Gilleland, A. T. Falls, J. Noraky, M. G. Heiman, and M. F. Yanik, "Computer-assisted transgenesis of *Caenorhabditis elegans* for deep phenotyping," *Genetics*, vol. 201, no. 1, pp. 39–46, 2015. [Online]. Available: http://www.genetics.org/content/201/1/39

[18] X. Dong, P. Song, and X. Liu, "An automated robotic system for high-speed microinjection of *Caenorhabditis elegans*," in *Proc. IEEE Int. Conf. Robot. Autom. (ICRA)*, May 2015, pp. 996–1001.

[19] P. Song, X. Dong, and X. Liu, "A microfluidic device for automated, high-speed microinjection of *Caenorhabditis elegans*," *Biomicrofluidics*, vol. 10, no. 1, Jan. 2016, Art. no. 011912.

[20] M. A. Unger, H.-P. Chou, T. Thorsen, A. Scherer, and S. R. Quake, "Monolithic microfabricated valves and pumps by multilayer soft lithography," *Science*, vol. 288, no. 5463, pp. 113–116, Apr. 2000.

[21] Y. Sun, S. Duthaler, and B. J. Nelson, "Autofocusing in computer microscopy: Selecting the optimal focus algorithm," *Microsc. Res. Technique*, vol. 65, no. 3, pp. 139–149, Oct. 2004.

[22] X. Y. Liu, W. H. Wang, and Y. Sun, "Dynamic evaluation of autofocusing for automated microscopic analysis of blood smear and pap smear," *J. Microsc.*, vol. 227, no. 1, pp. 15–23, Jul. 2007.

[23] T. Stiernagle, "Maintenance of *C. elegans*," in *WormBook*, Feb. 2006. [Online]. Available: http://www.wormbook.org, doi: 10.1895/wormbook.1.101.1.

[24] C. Juan, personal communication, Dec. 2014.

[25] X. Ai, W. Zhuo, Q. Liang, P. T. McGrath, and H. Lu, "A high-throughput device for size based separation of *C. elegans* developmental stages," *Lab Chip*, vol. 14, no. 10, pp. 1746–1752, 2014.

[26] I. D. C. Cáceres, N. Valmas, M. A. Hilliard, and H. Lu, "Laterally orienting *C. elegans* using geometry at microscale for high-throughput visual screens in neurodegeneration and neuronal development studies," *PLoS ONE*, vol. 7, no. 4, 2012, Art. no. e35037.

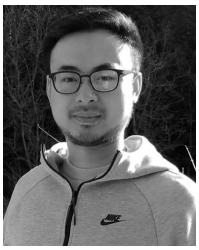

Xianke Dong received the bachelor's degree in control science and engineering from the Harbin Institute of Technology, Harbin, China, in 2012, and the Ph.D. degree in mechanical engineering from McGill University, Montreal, QC, Canada, in 2019.

He was a Visiting Mechanical and Industrial Engineer with the University of Toronto, Toronto, ON, Canada, from 2017 to 2019. He is currently a Computer Vision Research Scientist of convolutional neural network (CNN) with SR-Research Ltd., Toronto. His research involves a wide range of fields in robotics and artificial intelligence, such as biomedical robot and microrobot, robotic biomicromanipulation, system modeling and control, machine learning and deep learning, computer vision, and image processing.

Pengfei Song received the B.Eng. degree in mechanical engineering from Jilin University, Changchun, China, in 2013, and the Ph.D. degree in mechanical engineering from McGill University, Montreal, QC, Canada, in 2018.

He is currently a Lecturer and a Ph.D. Advisor with the Department of Electrical and Electronic Engineering, Xi'an Jiaotong–Liverpool University, Suzhou, China. His research interests lie primarily in micromaterials and nanomaterials/systems, which includes automated and high-throughput microfluidic systems for the model organism (e.g., *Caenorhabditis elegans*) studies, biosensors made from 2-D materials for affordable diseases diagnostics, and strain-engineered rolled-up nanostructures. He also has interests in microfluidic cell studies.

Dr. Song received several awards, including the Best Paper Award in Microfluidics Symposium at the 2014 ASME International Mechanical Engineering Congress and Exposition, the Best Conference Paper Award Finalist and the Best Automation Paper Award Finalist at the 2015 IEEE International Conference on Robotics and Automation (ICRA' 2015), and the Editors Pick Article Award and the Best Paper Award Finalist from *Biomicrofluidics* (AIP). He is also the China Scholarship Council (CSC) Award holder for his Ph.D. study in Canada.

Xinyu Liu (Member, IEEE) received the B.Eng. and M.Eng. degrees in mechanical engineering from the Harbin Institute of Technology, Harbin, China, in 2002 and 2004, respectively, and the Ph.D. degree in mechanical engineering from the University of Toronto, Toronto, ON, Canada, in 2009.

He is currently an Associate Professor and the Percy Edward Hart Professor with the Department of Mechanical and Industrial Engineering and is cross-appointed with the Department of Biomaterials and Biomedical Engineering, University of Toronto. Before joining the University of Toronto in September 2017, he was an Associate Professor and the Canada Research Chair in Microfluidics and BioMEMS with the Department of Mechanical Engineering, McGill University, Montreal, QC, Canada. His research interests include microrobotics, nanorobotics, and soft robotics, microfluidics, and BioMEMS.

Dr. Liu was a recipient of the Stars in Global Health Award from Grand Challenges Canada in 2012, the Douglas R. Colton Medal for Research Excellence from CMC Microsystems in 2013, the Christophe Pierre Award for Research Excellence from McGill University in 2017, and the Young Scientist Award from the Microsystems & Nanoengineering Summit in 2018. He is a Senior Editor of the IEEE ROBOTICS AND AUTOMATION LETTERS, and an Associate Editor of the IEEE TRANSACTIONS ON AUTOMATION SCIENCE AND ENGINEERING, the IEEE TRANSACTIONS ON NANOTECHNOLOGY, the *International Journal of Advanced Robotic Systems*, and the *IET Cyber-Systems and Robotics*, and has served on the Conference Editorial Boards of the three major IEEE Robotics and Automation Society Conferences (ICRA, CASE, and IROS).